Kobayashi et al. Progress in Earth and Planetary Science (2017) 4:6
DOI 10.1186/s40645-017-0124-y

Progress in Earth and Planetary Science

RESEARCH ARTICLE Open Access

High-resolution mapping and time-series measurements of ^{222}Rn concentrations and biogeochemical properties related to submarine groundwater discharge along the coast of Obama Bay, a semi-enclosed sea in Japan

Shiho Kobayashi[1*], Ryo Sugimoto[2], Hisami Honda[3], Yoji Miyata[4], Daisuke Tahara[2], Osamu Tominaga[2], Jun Shoji[5], Makoto Yamada[3], Satoshi Nakada[6] and Makoto Taniguchi[3]

Abstract

High-resolution mapping along the coast and time-series measurements of the radon-222 (^{222}Rn) concentrations in the shallow zone in a semi-enclosed sea, Obama Bay, Japan, were undertaken in 2013. The temporal and spatial variations in the ^{222}Rn concentrations were analyzed in parallel with meteorological conditions, physical–biogeochemical characteristics, and the submarine groundwater discharge (SGD) flux measured with a seepage meter. These data indicate that the groundwater influences the water properties of the bay and that the groundwater supply pathways are not limited to the local SGD. The concentrations of ^{222}Rn flowing into the bay from rivers was known to be relatively high because groundwater seeps from the river bed. High-^{222}Rn water was almost always present around the river mouth, and northward advection of the water affected the distribution of ^{222}Rn concentrations in the bay. The southward wind suppressed the advection of the high-^{222}Rn water and largely controlled the temporal variations in ^{222}Rn concentrations at a station located on the north side of the river mouth, whereas the local SGD affected the short-term changes in the ^{222}Rn concentrations. The concentrations of ^{222}Rn and chlorophyll-a, an indicator of phytoplankton biomass, show a significant positive correlation in the surface layer along the coastline in seasons when the nutrient supply was the main factor limiting primary productivity.

Keywords: Submarine groundwater discharge (SGD), ^{222}Rn monitoring, Chlorophyll-a, Nutrients, Wind-driven advection, Coastal seas

Introduction

It is challenging to obtain evidence of the effects of submarine groundwater discharges (SGDs) on marine ecosystems, partly because groundwater is an invisible source of the freshwater supplied to the sea. Fresh groundwater discharged from the sea bed often reduces the salinity of the bottom water and increases the concentrations of dissolved nutrients that are essential for primary producers. The correspondence between the low-salinity area associated with groundwater discharge and the high concentration of primary producers, such as benthic algae (Bruce 1925; Sanders 1979), seagrass (Kohout and Kolipinski 1967), and salt marsh plants (Nestler 1977), has been recognized since the 1920s. Based on those results, the ecological significance of groundwater discharge into coastal seas was discussed by Johannes (1980), but the distribution of salinity alone was an insufficient index with which to describe the

* Correspondence: shihok@kais.kyoto-u.ac.jp
[1]Field Science Education and Research Center, Kyoto University, Kitashirakawaoiwake, Sakyo-ku, Kyoto 606-8502, Japan
Full list of author information is available at the end of the article

influence of groundwater (Johannes 1980) because it does not distinguish SGD from other freshwater.

Since the 1980s, various methods have been developed to estimate the influence of SGD on marine primary production. The influence of SGD on primary producers and coastal ecosystems was quantified with the nitrogen budget method (Valiela and Costa 1988; Valiela et al. 1992). The effects of SGD on benthic microalgae and red tides were also quantified using the groundwater flow rate, which was calculated from the hydraulic gradient of groundwater on land (Campbell and Bate 1996; Laroche et al. 1997; Gobler and Sanudo-Wilhelmy 2001). A correspondence between the distributions of SGD and benthic microalgae was suggested with a visualization method using thermal imaging, based on the difference between the temperature of the seawater and that of SGD (Miller et al. 2004).

In recent years, the geochemical tracers radium and radon-222 (^{222}Rn) have been used to trace groundwater (Moore 1996; Burnett et al. 2006). ^{222}Rn is a short-lived radioisotope (half-life, 3.83 days) that is present in much higher concentrations in groundwater than in surface flow (Ellins et al. 1990). Using this powerful tracer, the influence of SGD on benthic microalgae was evaluated in the intertidal zone of the Yellow Sea (Waska 2011; Waska and Kim 2010). The nutrient fluxes caused by SGD and their potential effects on primary production have also been demonstrated in several coastal seas around Japan using ^{222}Rn (Shiokawa et al. 2013; Sugimoto et al. 2016).

A method of continuously monitoring the active concentrations of ^{222}Rn in water has been developed and used to visualize the distribution of groundwater in coastal seas (Burnett et al. 2001; Burnett and Dulaiova 2003). This method was first applied in tracking lines of over 100 km and successfully revealed the spatial distribution of SGD (Santos et al. 2008; Stieglitz et al. 2010). The applicability of this approach within a site of only a few kilometers in size was confirmed in a recent study using multiple ^{222}Rn detectors (Hosono et al. 2012).

SGD typically displays significant spatial and temporal variability (Burnett et al. 2006). Therefore, high-resolution mapping and time-series measurements of the ^{222}Rn concentrations and biogeochemical properties in the area of interest are required to quantify the influence of SGD on primary production along the coastline. In this study, we monitored the active concentrations of ^{222}Rn with multiple detectors from a boat (Stieglitz et al. 2010) to determine the distribution of ^{222}Rn concentrations in Obama Bay, Japan, within a study site of only a few kilometers in size (Fig. 1). We also monitored ^{222}Rn and the physical–biogeochemical properties of a site for a month and measured SGD directly with seepage meters (Lee 1977; Rutkowski et al. 1999; Taniguchi and Iwakawa 2004) to investigate the source of the ^{222}Rn. We then compared the distributions of SGD and chlorophyll-a (Chl-a), an indicator of the phytoplankton biomass. In Obama Bay, a correspondence between the high ^{222}Rn concentrations in the bottom layer and the elevated Chl-a concentrations were observed, suggesting that SGD influences phytoplankton growth (Honda et al. 2016). In this study, we investigated this relationship in more detail, focusing on the phytoplankton biomass in the shallow zone along the coastline.

Methods/Experimental

Study site

Obama Bay is a semi-enclosed embayment in Fukui Prefecture, Japan (Fig. 1a). The bay is one of the tributaries of Wakasa Bay, which is connected to the Japan Sea, and the tidal range is less than 20 cm. The surface area, volume, and mean depth of the bay are 58.7 km^2, 0.74 km^3, and 13 m, respectively. The annual precipitation in the watershed of Obama Bay is over 2000 mm/year. The discharge of two major rivers, the Kita and Minami rivers, is usually less than 10 m^3/s for each river between May and August (data on river discharge were provided by the Ministry of Land, Infrastructure, Transport and Tourism, Japan). There are significant groundwater resources in the basin, particularly on the Obama Plain (Sasajima and Sakamoto 1962), and there are more than 100 flowing artesian wells on this alluvial plain (Sugimoto et al. 2016).

The SGD rates (m^3/d) flowing into Obama Bay were estimated based on the monthly ^{222}Rn data and a steady-state mass balance model and were relatively high in spring (March–April), when snowmelt water was predominant, and in the rainy summer season (June–September) (Sugimoto et al. 2016). The annual mean concentration of ^{222}Rn in the river water flowing into Obama Bay was about 59.6 dpm/L, which was lower than that in the groundwater (mean 660 dpm/L) but was not negligible (Sugimoto et al. 2016).

The rainfall, snowfall, and wind velocity data, measured at the weather station designated “Obama” from 20 April to 15 May 2013, were obtained from the Automated Meteorological Data Acquisition System (AMeDAS) of the Japan Meteorological Agency. The mean monthly river discharge data from the largest river (Kita River) for 2013 were obtained from the Ministry of Land, Infrastructure, Transport and Tourism of Japan. The monthly changes in the meteorological conditions in 2013 are shown in Fig. 2. The total monthly rainfall was relatively high in January but gradually decreased and was lowest in May. It increased again in June and continued to be relatively high from June to August. It then increased markedly in September, which is the typhoon season. Significant snowfall was recorded in

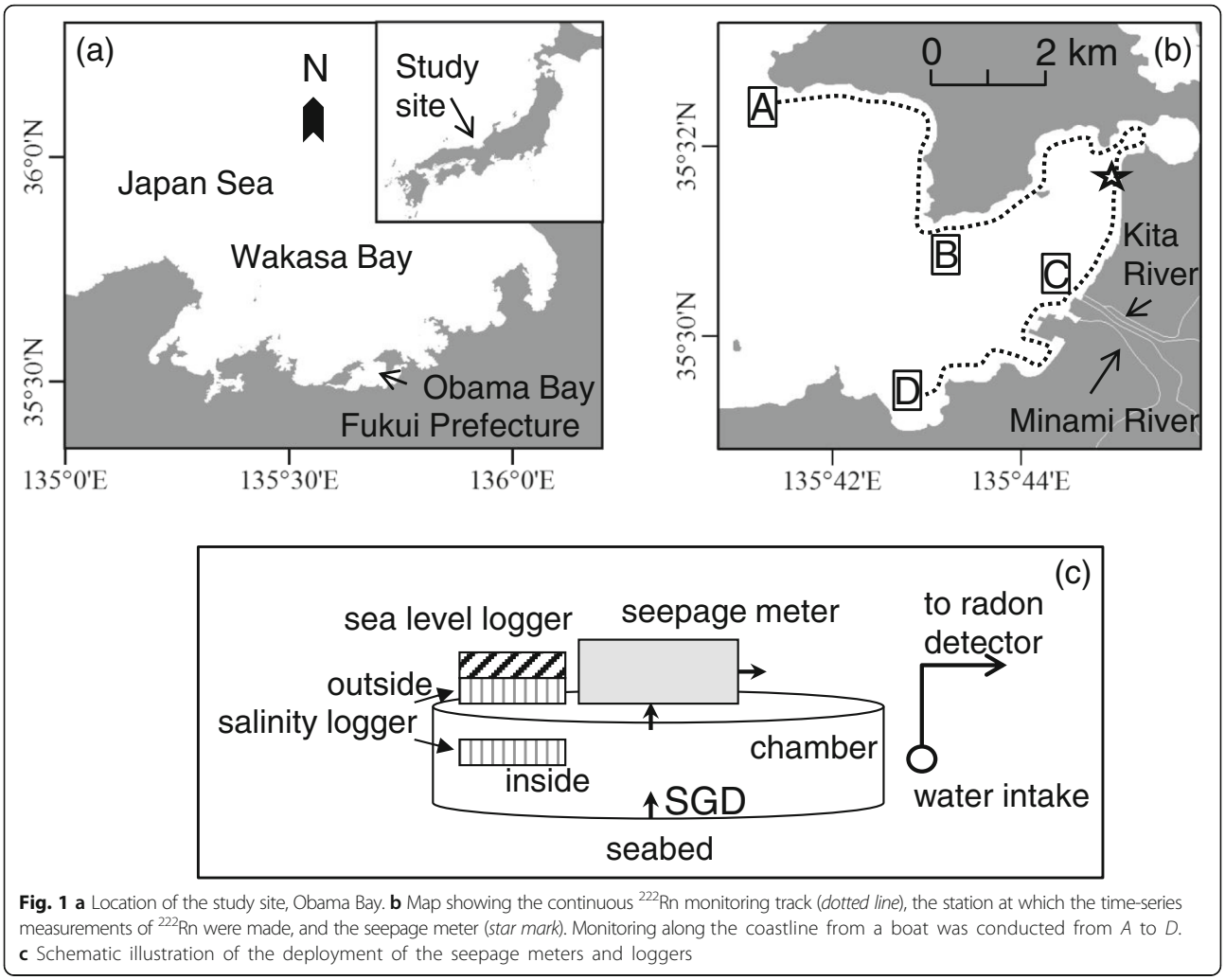

Fig. 1 **a** Location of the study site, Obama Bay. **b** Map showing the continuous ^{222}Rn monitoring track (*dotted line*), the station at which the time-series measurements of ^{222}Rn were made, and the seepage meter (*star mark*). Monitoring along the coastline from a boat was conducted from *A* to *D*. **c** Schematic illustration of the deployment of the seepage meters and loggers

winter (December to February). The mean monthly river discharge was relatively high from January to March, was lowest for the year in May, and increased slightly in June and July. It then increased markedly in September, when heavy rain fell in Obama City.

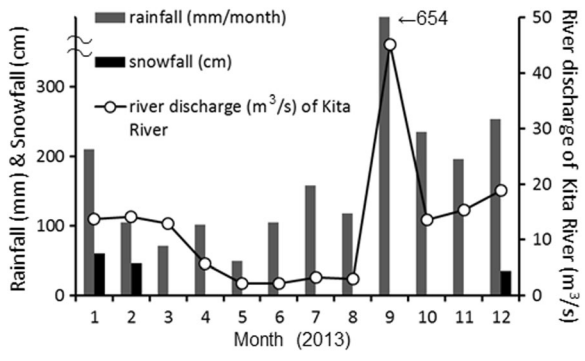

Fig. 2 Total monthly rainfall (mm) and snowfall (cm) and mean monthly river discharge rate of the Kita River (m^3/s) in 2013

Measurements and sampling

The distributions of the ^{222}Rn concentrations along the eastern coast of Obama Bay were measured on 13, 15, and 16 March, 7 June, 22 July, and 12 September, 2013, with electronic Rn detectors (RAD 7: Durridge) from a research boat belonging to Fukui Prefectural University. The boat ran close to the coast, within 10 m of land, where the depth of the water column was around 2 m, at a speed of 1–2 knots. The tracking line is shown in Fig. 1a. Monitoring was conducted from Tomari (A) to Seihama (D). The total distance of the tracking line was about 15 km.

Seawater was pumped at 5–10 L/min from 0.5 m below the surface, and the temperature and salinity of the water were measured every 1 min using a CTD instrument (AAQ1183: JFE-Advantech). The ^{222}Rn in the seawater was measured and analyzed according to Stieglitz et al. (2010), who developed an Rn detector system which consists of three Rn detectors connected in parallel and interfaced with an air–water exchanger (Dulaiova et al. 2005). We used two sets of Rn detector

systems, with a measurement interval for each system of 10 min, so the average values and standard deviations of the ^{222}Rn concentrations were obtained every 5 min. Seawater samples for analyses of nutrient concentrations and Chl-a were collected every 10 min and every 20 min, respectively. However, seawater sampling for analyses of Chl-a failed at some points in March.

At a station on the tracking line (star in Fig. 1b), we measured the temporal variations in the ^{222}Rn concentrations in addition to the SGD fluxes, using a seepage meter. The water depth at the station was around 1 m. Divers deployed the seepage chamber (base radius, 15 cm) on the seabed at the station on 18 April 2013. A diagram of the seepage chambers is shown in Fig. 1c. Salinity and temperature loggers (Infinity-CT or MDS-CT, JFE-Advantec) were set inside and outside the chambers, whereas sea-level loggers (DIK-613A, Daikirika) were set only on the outsides of the chambers. The details of the seepage meters have been described by Taniguchi and Iwakawa (2004). We calibrated the seepage meters in the laboratory with a Coriolis flowmeter (FD-S, Keyence) before and after the field measurements were made. The seepage fluxes were determined in mL/min from each calibration curve and then converted to cm/d using the area of the chambers (cm^2). Seawater was pumped from the sea bottom at 5–10 L/min next to the chamber (Fig. 1c) from 20 April to 15 May in 2013. The ^{222}Rn concentrations in the seawater were measured every 10 min using a ^{222}Rn detector (RAD 7: Durridge) interfaced with an air–water exchanger located on land. The seawater samples for nutrient analysis were collected once a day from 20 April to 12 May in 2013. The times of water sampling are shown with the data on nutrient concentrations (Fig. 10).

Samples and data analysis

The seawater samples were filtered through GF/F 0.7 μm glass filters, frozen, and stored in the freezer. The concentrations of nitrate (NO_3), nitrite (NO_2), phosphate (PO_4), and dissolved silicate (DSi) were measured with an auto-analyzer (QuAAtro, BL-Tech). The concentration of ammonium (NH_4) was measured with a fluorometer (Trilogy, Turner Design) with a CDOM/NH4 module (Model 7200-041, Turner Design), using the ortho-phthaldialdehyde (OPA) method (Holmes et al. 1999). In this study, we defined dissolved inorganic nitrogen (DIN) as the sum of NO_3 and NO_2 because almost all the concentrations of NH_4 at the surface along the coastline were below the detection limit (0.1 μM). Dissolved inorganic phosphorous (DIP) is defined as PO_4. The concentration of Chl-a on the GF/F filters was quantified with a calibrated fluorometer (Trilogy, Turner Design). The analytical errors were within 10%, suggesting that the values analyzed were sufficiently accurate to draw conclusions from the data.

For the data analysis, we used the ^{222}Rn concentrations in the river water flowing into the bay, which had been measured monthly in 2013 by Sugimoto et al. (2016). Because approximately 80% of the riverine ^{222}Rn entering the bay is contributed by the two major rivers (Kita and Minami rivers), the mean ^{222}Rn concentrations in the two rivers were assumed to represent the value for the surface river waters (Sugimoto et al. 2016). We also used the ^{222}Rn concentrations and salinity in the terrestrial groundwater measured in March 2013 by Sugimoto et al. (2016).

The temporal changes in the tidal level from 20 April to 15 May 2013 were also obtained from the Japan Meteorological Agency. We used fast Fourier transforms (FFTs), providing power spectra, to evaluate the fluctuation cycles in the time series for wind velocity, sea level, SGD flux, and ^{222}Rn concentration.

We evaluated the factors limiting primary productivity using the equations of Steel (1962) for temperature (F_T) and nutrients (F_N), as follows:

$$F_T = T/T_{opt} \times \exp\left(1-T/T_{opt}\right) \quad (1)$$

$$F_N = \mathrm{MIN}\left(\mathrm{DIN}/(K_N + \mathrm{DIN}),\ \mathrm{DIP}/(K_P + \mathrm{DIP})\right) \quad (2)$$

where T_{opt} (25 °C) is the optimum temperature for phytoplankton growth, and K_N (1.7 μM) and K_P (0.19 μM) are the half-saturation constants for DIN and DIP, respectively. These parameters were obtained from studies of the Japanese coast (Yanagi and Onitsuka 1999). We set T, DIN, and DIP to the maximum and minimum values extracted from the temperatures, DIN concentrations, and DIP concentrations observed in each month, respectively.

Results and Discussion

Distributions of the concentrations of ^{222}Rn, nutrients, and Chl-a along the coastline

High-resolution mapping of ^{222}Rn was performed in March, June, July, and September of 2013. The concentrations of ^{222}Rn, salinity, and Chl-a along the coastline in each month are shown in Figs. 3, 4, and 5, respectively. For the purpose of illustration, the tracking line was divided into three zones by four points (A–D, shown in Fig. 1b). The results of ^{222}Rn mapping show common patterns in the spatial distributions during June, July, and September: the concentrations were relatively high in the zone between B and D but low in the zone between A and B (Fig. 3). The concentration in the zone between C and D was highest in July. The average concentrations of ^{222}Rn on the tracking line (from A to D) in June, July, and September were nearly equal, at 2.8, 3.3, and 2.6 dpm/L, respectively. The average concentration of ^{222}Rn in March was 9.6 dpm/L, much higher than in the other 3 months. The distribution of

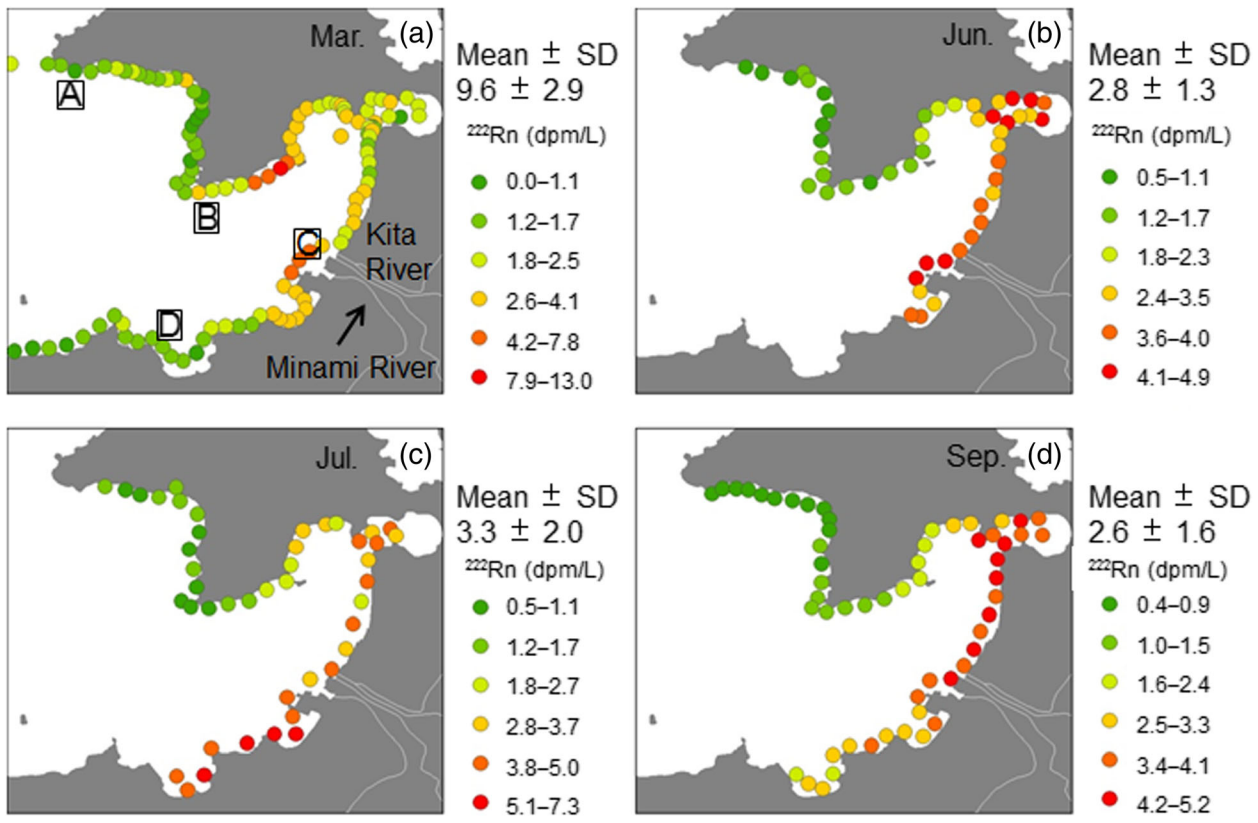

Fig. 3 Distributions of ^{222}Rn (dpm/L) in **a** March, **b** June, **c** July, and **d** September, determined by monitoring the coastline from a boat. All the data in March are shown in the same panel, although each datum was obtained on a different day

the ^{222}Rn concentration in March differed from that in the other months. The ^{222}Rn concentration was highest around point B but relatively low in the zone between B and C.

In June, July, and September, salinity was relatively low in the zone between B and D but high in the zone between A and B (Fig. 4). The distributions of low-salinity water corresponded strongly to the zones in which the ^{222}Rn concentrations were relatively high in all surveys. The distribution of Chl-a was constant throughout the survey, including in March. The Chl-a concentrations were relatively high in the zone between B and D but low in the zone between A and B (Fig. 5). The distribution of high-Chl-a water corresponded strongly to the zones in which the ^{222}Rn concentration was relatively high.

The correspondence between the distributions of ^{222}Rn and Chl-a is shown in Fig. 6. The distributions of both parameters corresponded well in June, July, and September, but not in March. The locations of the peak values for the two parameters differed in March. The correlation coefficients indicated significant correlations between the concentrations of ^{222}Rn and Chl-a in June, July, and September. Significant correlations were also obtained between the concentrations of ^{222}Rn and PO_4 in June and between salinity and NO_3 in March, June, and September (Table 1).

We created the zones shown in Fig. 1b using points A–D to investigate the differences in the biogeochemical properties of each zone along the coastline. The datasets obtained from all the observations made in March, June, July, and September were integrated, and the average concentrations of ^{222}Rn, salinity, NO_3, and PO_4 in each zone are shown in Fig. 7. In the zone between A and B, salinity was relatively high and the concentrations of ^{222}Rn, NO_3, and PO_4 were low. Salinity was lowest and the concentration of NO_3 was highest in the zone between B and C, whereas PO_4 was not high in this zone. The concentrations of ^{222}Rn and PO_4 were highest in the zone between C and D.

Temporal changes in the concentration of ^{222}Rn, SGD flux, and biogeochemical properties

Figure 8 shows temporal variations in the ^{222}Rn concentration measured with a Radon detector; the SGD flux measured with a seepage meter, the wind velocity (a parameter of the physical environment), and salinity levels inside and outside the seepage chamber at the point at

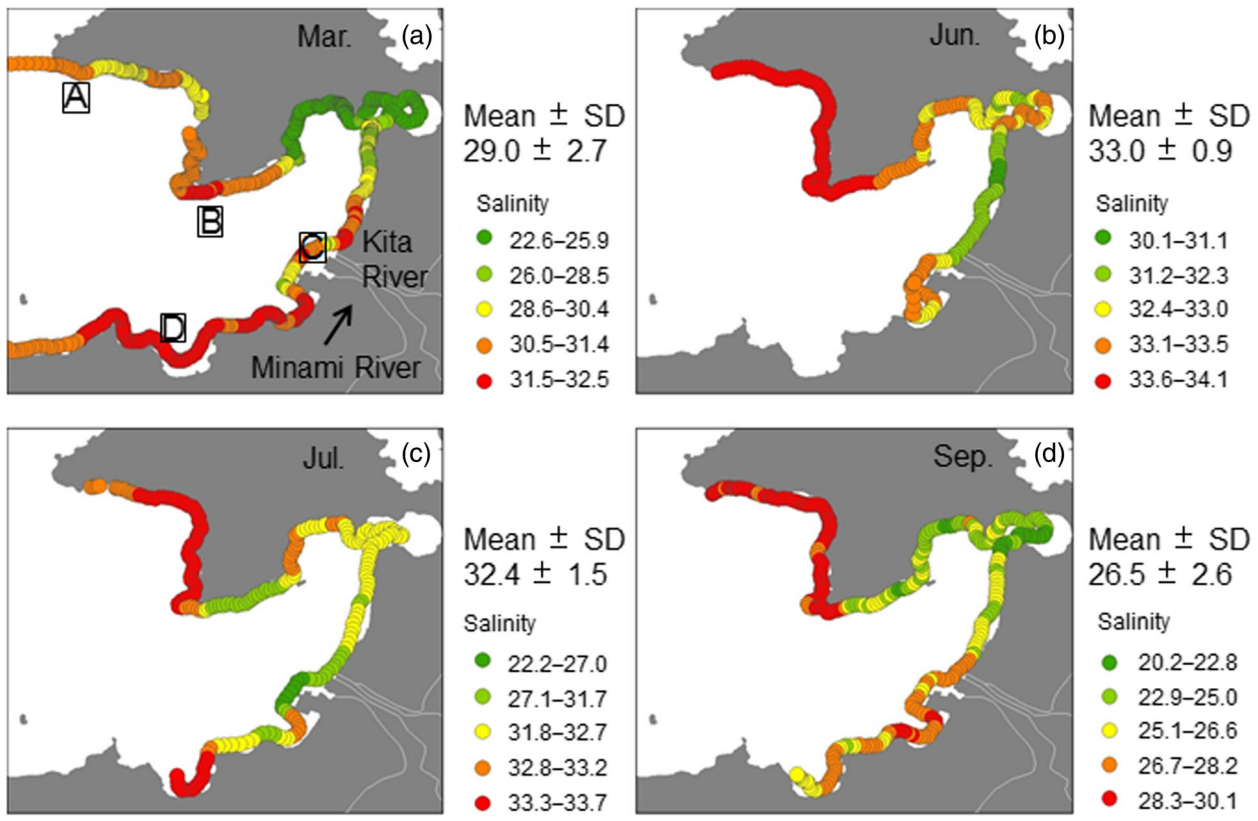

Fig. 4 Distributions of salinity in **a** March, **b** June, **c** July, and **d** September, determined by monitoring the coastline from a boat. All the data in March are shown in the same panel, although each datum was obtained on a different day

which the ^{222}Rn concentration was relatively high (star; location shown in Fig. 1b). The sea level varied from 0.7 to 1.2 m. The concentrations of ^{222}Rn increased and decreased over a 5–6 day cycle, although the SGD flux showed no such cycle (Fig. 8a). The minimum values of the cycle were nearly stable from April to May, whereas the SGD flux dropped sharply to almost zero in May. Figure 9 shows the FFT power spectra for the SGD flux, the sea level at the station, the concentration of ^{222}Rn, and the wind velocity and salinity inside and outside the chamber. The power spectrum for the SGD flux shows variations with diurnal (25 h) and semidiurnal (12.5 h) cycles, with characteristics similar to those of the power spectrum for sea level. The temporal variations in the ^{222}Rn concentrations throughout the monitoring period showed a 5–6 day cycle and were coincident with those in the wind velocity; ^{222}Rn increased when the northward wind became strong but decreased when the southward wind became dominant (Fig. 8b). The results of the FFT analysis also revealed that ^{222}Rn and wind velocity peaked with a periodicity of ~100 h (Fig. 9). As for the shorter cycles, the power spectra for wind, salinity, and the concentration of ^{222}Rn displayed peaks with periodicities of 24, 20–24, and 20 h, respectively.

Figure 8c shows the temporal variations in salinity inside and outside the chamber. The salinity outside the chamber shows negative peaks, with the period of low salinity ranging from 1 to 7 h. Peaks were observed almost daily, whereas no peaks occurred between 24 and 26 April, from 30 April to 3 May, or between 6 and 9 May. Several peaks coalesced into a single peak on 26–27 April. The salinity inside the chamber also showed negative peaks 6–12 h after the negative peaks in the outside salinity, although the magnitude of the declines was much smaller than the declines in the outside salinity. The inside salinity also displayed a declining trend in April and an increasing trend in May.

The temporal variations in salinity outside the chamber are presented with the wind velocity data (Fig. 8d). The northward wind showed peaks over a 5–6 day cycle. The negative peaks in the outside salinity appeared 5–6 h after the northward wind strengthened. The outside salinity remained high during periods when the southward wind was dominant.

Temporal variations in the concentrations of nutrients (NO_3, PO_4, DSi) and associated biogeochemical properties at the station described above are shown in Fig. 10. The plots in Fig. 10a indicate the times of water

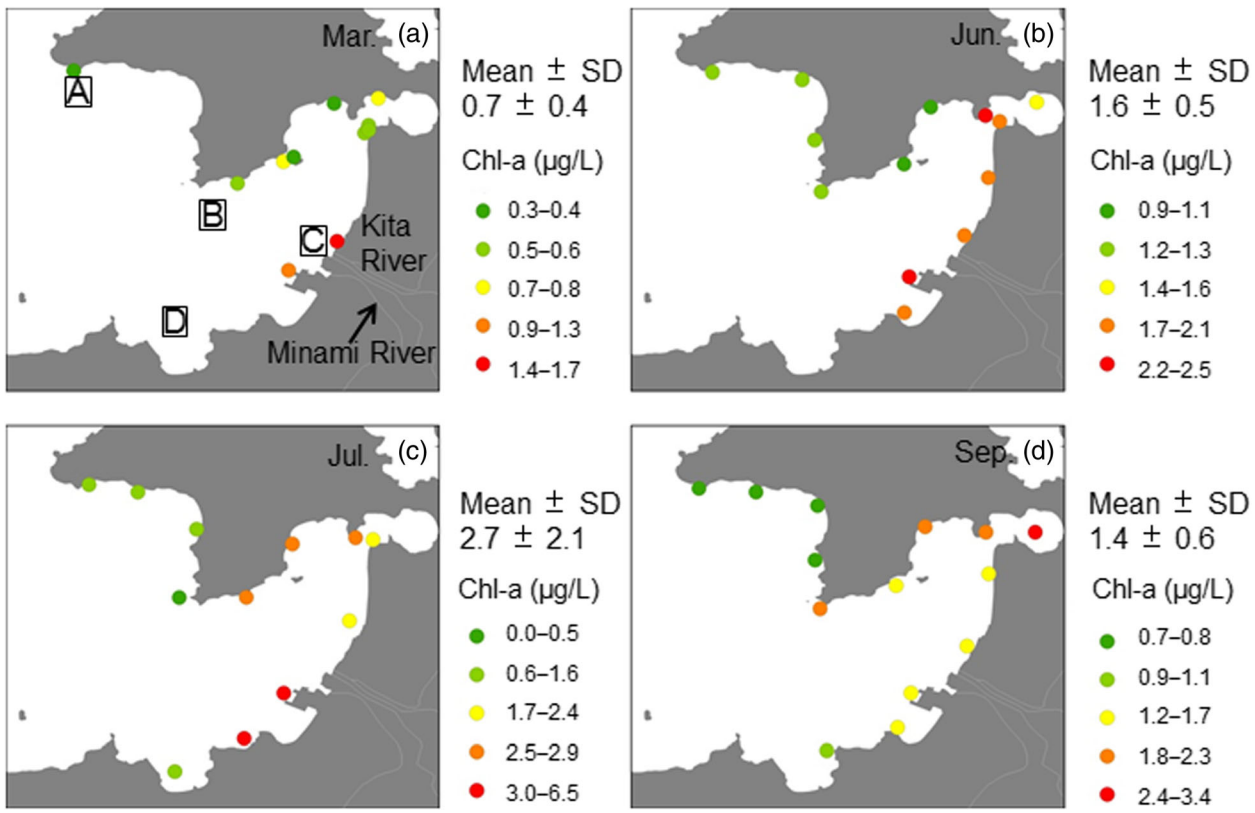

Fig. 5 Distributions of chlorophyll-a (μg/L) in **a** March, **b** June, **c** July, and **d** September, determined by monitoring the coastline from a boat. All the data in March are shown in the same panel, although each datum was obtained on a different day

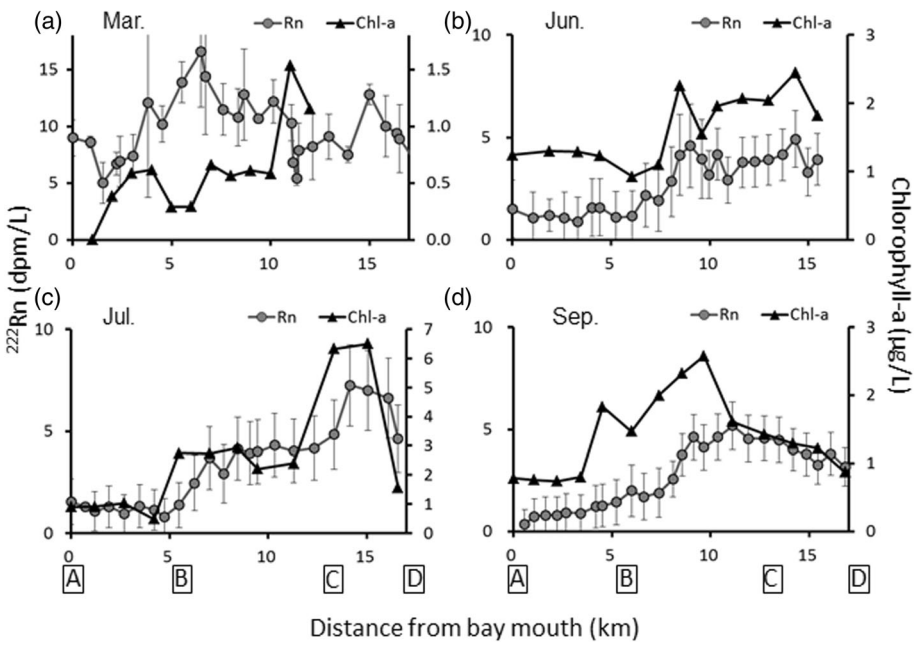

Fig. 6 Line plots of ^{222}Rn (dpm/L) and chlorophyll-a (μg/L) in **a** March, **b** June, **c** July, and **d** September, observed by monitoring the coastline from a boat. Letters *A* to *D* in **c** and **d** correspond to those in Fig. 1b

Table 1 Correlation coefficients for salinity and nutrients, ^{222}Rn and nutrients, and ^{222}Rn and chlorophyll-a

	Sal. vs. NO_3	Sal. vs. PO_4	^{222}Rn vs. NO_3	^{222}Rn vs. PO_4	^{222}Rn vs. Chl-a
March, 2013	−0.76**	0.12	0.37*	0.18	−0.17
June, 2013	−0.66**	−0.15	0.14	0.54**	0.91**
July, 2013	−0.35	−0.11	−0.12	0.37	0.79**
September, 2013	−0.82**	0.10	0.38	0.29	0.52*

Significant correlations are marked with asterisks
**Significant ($p < 0.01$) *significant ($p < 0.05$) *no mark* not significant
Sal. salinity, *vs.* versus

sampling for nutrient analysis. The ^{222}Rn concentrations at the daily sampling times were extracted from Fig. 8a and are plotted in Fig. 10b. The tide level shows diurnal (25 h) and semidiurnal (12.5 h) cycles, but the timing of water sampling was not related to the tidal cycle. The concentrations of PO_4 varied between 0.1 and 0.2 μM and increased and decreased over a 5–6 day cycle. The concentration of DSi ranged between 0.0 and 6.4 μM and showed several relatively large peaks that lasted for 1–2 days during the monitoring period. The concentrations of NO_3 ranged between 0.0 and 1.0 μM and peaked on the days when DSi increased. The temporal variations in the concentrations of PO_4 throughout the monitoring period showed a weak relationship with the daily average concentrations of ^{222}Rn ($r = 0.27$, $p = 0.1$), whereas the changes in NO_3 and DSi showed no relationship to the changes in ^{222}Rn.

Distribution of ^{222}Rn concentrations and its source

The concentrations of ^{222}Rn at the northern end of the tracking line, the point closest to the outside of the bay, were less than 1.5 dpm/L throughout the sampling period (Fig. 3), confirming that the influence of SGD was infrequent. In contrast, high ^{222}Rn concentrations (up to 15 dpm/L) were observed inside the bay throughout the monitoring period, suggesting the influence of SGD in Obama Bay.

The average ^{222}Rn concentration was highest in March (9.6 ± 2.9 dpm/L), whereas the values in June, July, and September (2.8 ± 1.3, 3.3 ± 2.0, and 2.6 ± 1.6 dpm/L, respectively) were relatively low. The average salinity in March was 29.0 ± 2.7, much lower than outside the bay at the end of February (33.3; Sugimoto et al. 2016). The average salinity was lowest in September (26.5 ± 2.6) in

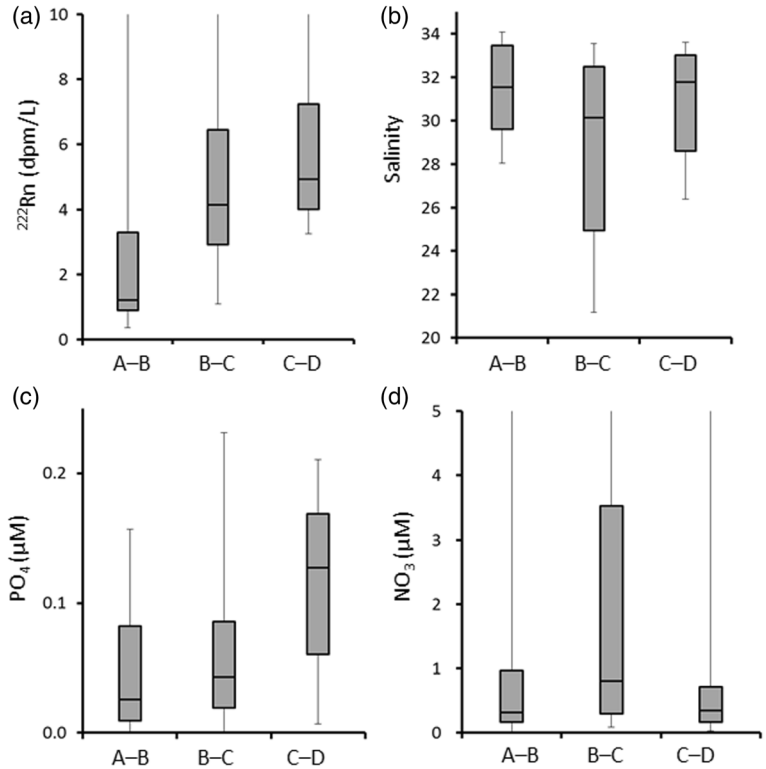

Fig. 7 Box plots of **a** ^{222}Rn (dpm/L), **b** salinity, **c** phosphorous (μM), and **d** nitrate (μM), showing the minimum and maximum values, 25th and 75th percentiles, and median values, from data obtained by monitoring the coastline from a boat in March, June, July, and September

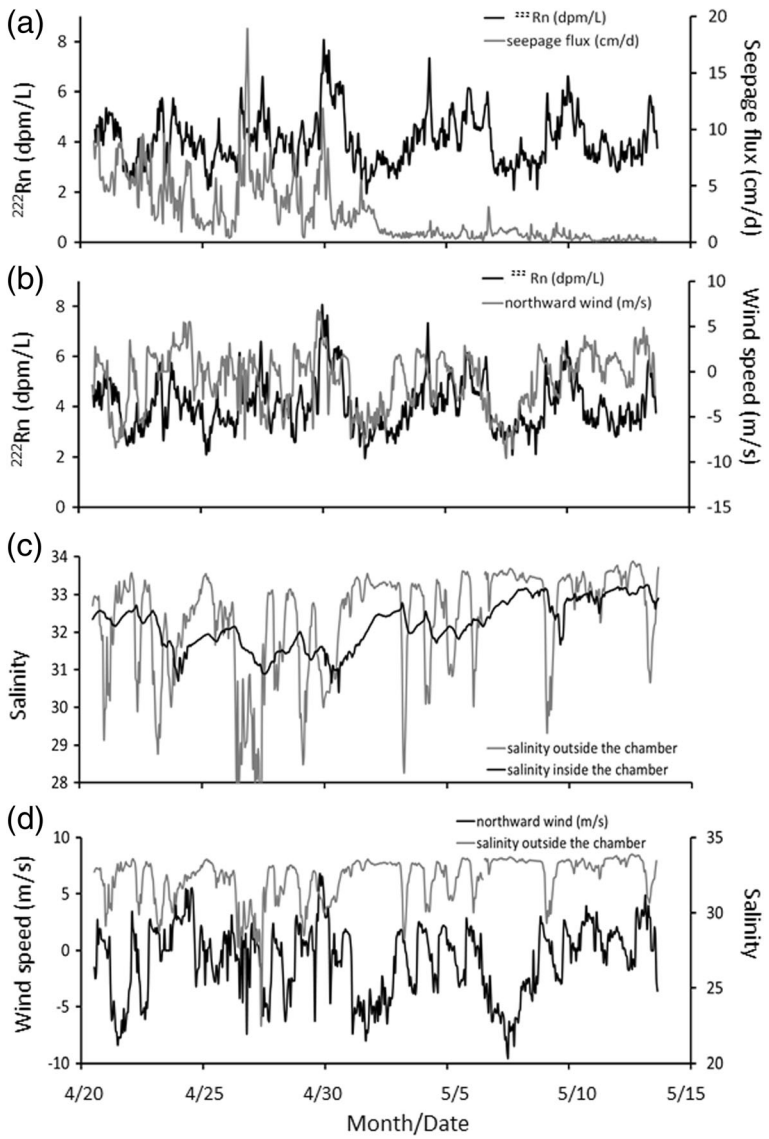

Fig. 8 Time series of **a** ^{222}Rn (dpm/L) and SGD fluxes measured with a seepage meter (cm/d), **b** ^{222}Rn (dpm/L) and northward wind (m/s), **c** salinity inside and outside the chamber, and **d** northward wind (m/s) and salinity outside the chamber, observed at a fixed station (*star*, shown in Fig. 1b) from 20 April to 15 May, 2013. The wind velocity data were obtained from AMeDAS

response to heavy typhoon rain. The river discharge was relatively high and largely stable from January to March, suggesting the influence of snowmelt water after significant snowfall in January and February (Fig. 2). These results are consistent with those of Sugimoto et al. (2016), who reported that the SGD rates flowing into Obama Bay, estimated from monthly ^{222}Rn data with a steady-state mass balance model, were relatively high in spring (March–April) when snowmelt water was the highest.

The ^{222}Rn concentration was measured along a few kilometers of the coastline every 5 min in this study, using two sets of a three-radon-detector system at a boat speed of 1–2 knots. The spatial resolution was slightly higher than that in previous pioneering works (Stieglitz et al. 2010; Hosono et al. 2012), and the distribution of the ^{222}Rn concentration along the coast of the semi-enclosed bay was determined in detail. Similar distributions were observed in June, July, and September, when the ^{222}Rn concentration was highest around the mouths of the Kita and Minami rivers, and the high-^{222}Rn water dispersed along the eastern coast toward the north (Fig. 3).

The first candidate source of high-^{222}Rn water is the river water. The ^{222}Rn concentrations in the river water collected at the river mouths in Obama Bay were relatively high (maximum, 234 dpm/L; Sugimoto et al. 2016) because groundwater seeps from the river bed and then flows rapidly down to the river mouth. These concentrations are consistent with those at other river mouths in

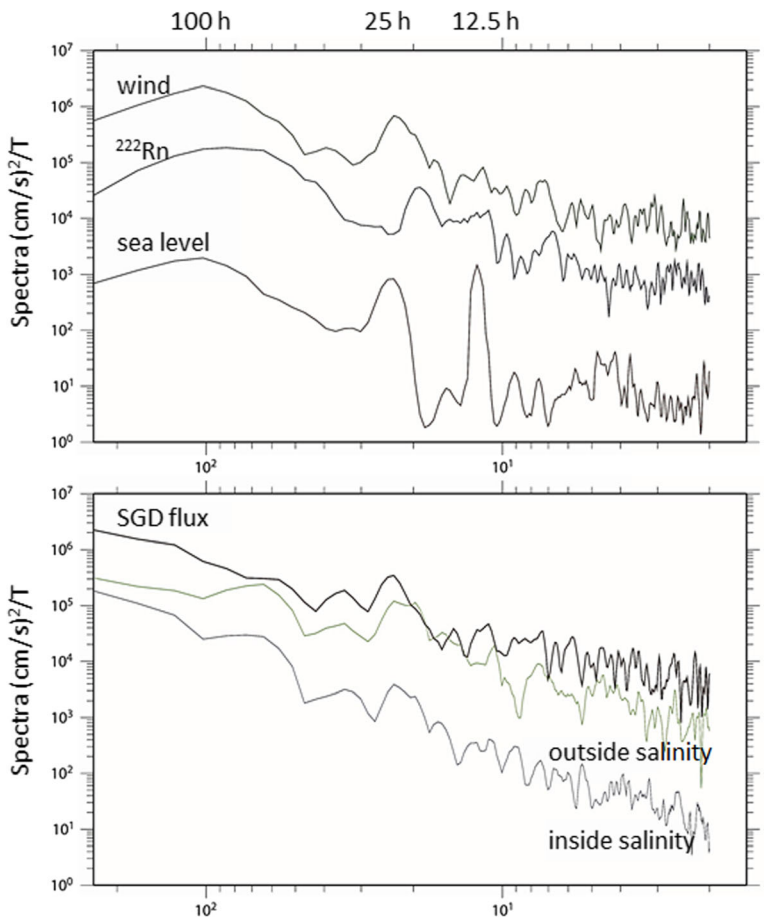

Fig. 9 Spectra obtained with fast Fourier transforms (FFTs) for the time series of ^{222}Rn, SGD flux, sea level, and salinity outside and inside the chamber, observed at a fixed station (*star* in Fig. 1b) from 20 April to 15 May 2013. The northward wind data were obtained from AMeDAS

Japan (e.g., Hosono et al. 2012; Shiokawa et al. 2013), whereas those at the mouths of continental rivers are much lower (e.g., Cable et al. 1996). The total river discharge was large enough (approximately 1.0–2.0 × 10^6 m^3/day; Sugimoto et al. 2016), and the axis of the bay was small enough (<4 km) for the river water to disperse throughout the bay within the period of ^{222}Rn degradation (half-life, 3.83 days).

The second candidate source of high-^{222}Rn water is the relatively large SGD offshore from the mouths of the Kita and Minami rivers, as has been mentioned in other surveys conducted by Obama City and models of the flow streams of terrestrial groundwater in the watersheds. Interviews with local residents confirmed the presence of fresh SGD at the point. However, we could not access the sites at the mouths of the Kita and Minami rivers to deploy seepage meters at that time. The concentrations of PO_4 and ^{222}Rn were both highest along the coastline and correlated with one another (Fig. 7; Table 1) around this site (in the zone between C and D, see Fig. 1b), indicating the presence of significant SGD.

Temporal changes in ^{222}Rn concentration and SGD flux

We continuously monitored the concentration of ^{222}Rn and measured the SGD flux using a seepage meter at a specific station (location shown in Fig. 1b) for a month, to determine the major sources of ^{222}Rn. The seepage meter located on the sea bottom indicated the presence of local SGD at the station (Fig. 8a). SGD includes the submarine fresh groundwater discharge (SFGD), originating from the freshwater on land, and the recirculated submarine groundwater discharge (RSGD), originating from the seawater that infiltrates the seabed under tidal influences (Taniguchi 2002a; Taniguchi et al. 2002b). The SFGD and RSGD generally show large differences in salinity, so they can be separated. We calculated them using the salinity inside and outside the chamber, as shown in Fig. 8c. The contribution rate of fresh SGD (SFGD/SGD × 100 [%]) was calculated as follows (Ishitobi et al. 2007):

$$\mathrm{SGD} = \mathrm{SFGD} + \mathrm{RSGD} \tag{3}$$

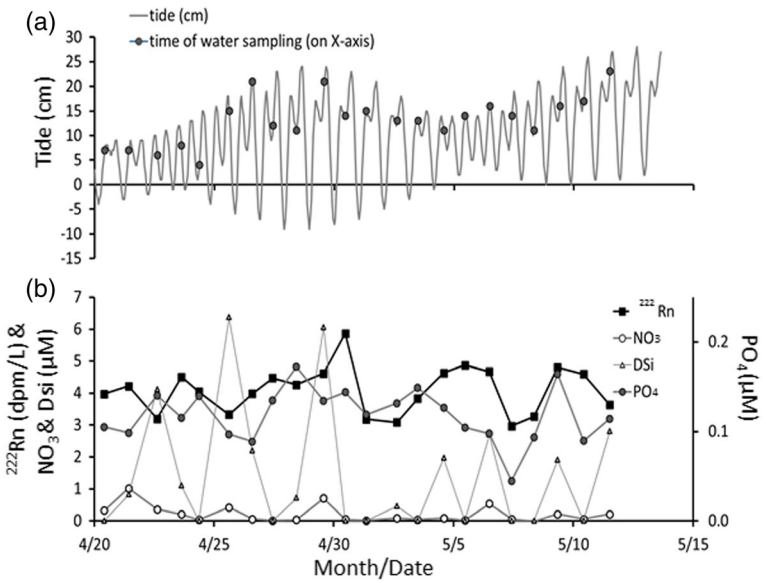

Fig. 10 As in Fig. 8 but for **a** tidal level (m) and the concentrations of **b** ^{222}Rn (dpm/L), phosphorous (μM), nitrate (μM), and silicate (μM). Values on the *X*-axes of the plots in **a** indicate the time (h) of water sampling for nutrient analysis, and those on the *Y*-axes of the plots are the tide levels at those times

$$\mathrm{SGD} \times C_{\mathrm{sgd}} = \left(\mathrm{SFGD} \times C_{\mathrm{sfgd}}\right) + \left(\mathrm{RSGD} \times C_{\mathrm{rsgd}}\right) \quad (4)$$

where SGD is the seepage flux determined with a seepage meter, C_{sgd} is the salinity inside the chamber, C_{rsgd} is the salinity outside the chamber, and C_{sfgd} is the salinity of the fresh groundwater on land. In this study, C_{sfgd}, which is the salinity (calculated from conductivity measurements) of the terrestrial groundwater calculated by Sugimoto et al. (2016), was assumed to be zero. The level of SGD flux changed sharply on 1 May, so we divided the datasets for SGD flux and salinity into the periods 20 April–1 May and 2–15 May. C_{rsgd} was set to the salinity averaged over each period, and C_{sgd} was set to the salinity averaged over the 1 h before the end of each period. We then solved the system of equations to calculate SFGD and RSGD. When C_{sgd} was larger than C_{rsgd}, the contribution of SFGD was assumed to be zero.

The contribution rates of SFGD (%) varied among months at the station: 1.4% in April but 0.0% in May 2013. The average SGD flux was 4.6 cm/day in April and 0.8 cm/day in May, with minimum and maximum values for the whole monitoring period of 0.1 and 18.9 cm/day, respectively. The average SGD fluxes were smaller than the results in the Chokai area (average SGD flux = 38.9 cm/day; Hosono et al. 2012), where the tidal range is as small as that in Obama Bay, but large SFGD fluxes were observed. The average SFGD flux, 0.41 cm/day, was consistent with that obtained with the ^{222}Rn mass balance model throughout the bay (0.62 cm/day; Sugimoto et al. 2016).

Temporal changes in the SGD flux and sea level showed variations with diurnal (25 h) and semidiurnal (12.5 h) cycles (Fig. 9), suggesting the influences of diurnal and semidiurnal tides. This indicates that the SGD at the site consisted mainly of tidally influenced RSGD. The observed SGD flux dropped sharply to almost zero, and the salinity inside the chamber increased in May, while the seasonal change in the SGD flux was consistent with that obtained with the ^{222}Rn mass balance model (Sugimoto et al. 2016). These trends indicated that the reduced SGD flux in May was partly attributable to the disappearance of the snowmelt water and partly to the rise in sea level from May, when SGD was suppressed. The seasonal changes in snowmelt water and sea level are mainly attributed to the seasonal change in air temperature, which varies little from year to year. These factors may explain the reduction in SGD observed in this study.

The minimum values of the 5–6 day cycle of the ^{222}Rn concentration were almost constant from April to May, whereas the local SGD flux observed at the station dropped sharply in May (Fig. 8), suggesting the influence of the advection of high-^{222}Rn water. The observed distribution of the ^{222}Rn concentration along the coast suggested that high-^{222}Rn water was present around the mouths of the Kita and Minami rivers during the observation period (Fig. 3). The results of the FFT analysis (i.e., that both the ^{222}Rn concentration and wind velocity showed peaked with a periodicity of ~100 h; Fig. 9) indicated that wind played an important role in the advection of high-^{222}Rn water.

We estimated the time (T_i) required for the high-^{222}Rn water near the mouths of the Kita and Minami rivers to reach the station. As an example, for the northward wind velocity of ~2 m/s that prevailed for 6 h daily between 2 and 13 May (Fig. 8), the velocity of the wind-driven flow, V (m/s), was calculated as follows:

$$V = \mathrm{ro\_a} \times \mathrm{C_d} \times \mathrm{W\_y} \times \sqrt{\mathrm{W\_x^2 + W\_y^2}/\mathrm{ro\_s} \times \mathrm{dt/dz}} \quad (5)$$

where ro_a is the density of air, C_d is the friction coefficient at the sea surface, ro_s is the density of seawater, and W_x and W_y are the wind velocities along the X- and Y-axes, respectively. We set the Y- and X-axes to north–south and west–east, respectively; dt is the time scale on which the wind blows in a particular direction and dz is the friction depth. The friction depth (D) was defined as follows (Officer 1976):

$$D = \pi \sqrt{2 * \ N_z/f} \quad (6)$$

where π is 3.14, f is the Coriolis coefficient (7.3×10^{-5}) at latitude 35° north, and N_z is the eddy viscosity coefficient. D ranges from 5 to 50 m, assuming N_z ranges from 1 to 100 cm^2/s. The minimum value of D exceeds the water depth of the coastal zone of the bay, so we set dz to equal the water depth of 1–5 m. We assumed the following values: ro_a, 1.205 kg/m^3; C_d, 0.0013; ro_s, 1022 kg/m^3; W_x, zero; W_y, 2 m/s; and dt, 6 × 3600 s.

Using equation (5), the resulting V value is 0.03–0.13 m/s. We would expect the actual flow speed to be higher than this value because of the additional influence of the density-driven flow. Because the distances between the river mouths and the station were ~2 km, T_i is less than 1.0 day, which is much shorter than the half-life of ^{222}Rn (3.83 days). Therefore, the high-^{222}Rn water near the mouths of the Kita and Minami rivers is a potential source of ^{222}Rn in the area of the station.

Influence of the advection of high-^{222}Rn water on ^{222}Rn concentrations

The results of the FFT analysis indicated that both the ^{222}Rn concentration and the wind velocity peaked with a periodicity of ~100 h (Fig. 9), suggesting that wind was strongly related to the long-term temporal changes in the ^{222}Rn concentration at the observation site. In this section, we examined the influences of the advection of high-^{222}Rn water, caused by wind, on temporal changes in the concentrations of ^{222}Rn in more detail.

In the short term, the temporal changes in the wind, salinity, and ^{222}Rn concentration displayed variations with periods of around 24, 20–24, and 20 h, respectively (Fig. 9). Therefore, the cycle of the ^{222}Rn concentration was not perfectly coincident with the variations in wind velocity. This is considered to be partly because the advection of the low-salinity high-^{222}Rn water within a day was controlled not only by the wind but also by the tidal currents, the density flow (such as the estuarine circulation), vertical mixing, and the interactions of all these factors, and partly by the technological limitations of the FFT analysis, which were attributed to the spike-like changes in salinity and the ^{222}Rn concentration. Therefore, the temporal variation in salinity was mainly controlled by wind, in addition to many physical factors, and the temporal variation in the ^{222}Rn concentration could be synchronized to that in salinity.

The salinity at the station increased during the periods when the southward wind was dominant (Fig. 8d), suggesting that the northward dispersion of the low-salinity high-^{222}Rn water flowing from the mouths of Kita and Minami rivers was suppressed. The 1 h averaged ^{222}Rn concentrations, measured every 10 min at the station (location indicated by a star in Fig. 1b), are plotted versus salinity outside the chamber in Fig. 11, to allow a discussion of the influence of wind.

The northward wind was dominant on 30 April and then weakened on the next day. The southward wind became strong on 2 May (Fig. 8d), so we used the datasets for the ^{222}Rn concentration and salinity in the period 30 April–2 May. The endmembers and mixing curves are shown in Fig. 11a, and the data for the 3 days in this period, which were measured from noon on 1 day to noon on the next day, are plotted in Fig. 11b, along with a part of each mixing curve. The ^{222}Rn concentration and salinity of seawater outside the bay, measured on 26 April 2013, were 0.9 dpm/L and 34.0, respectively. The ^{222}Rn concentrations measured on the same date in the two major rivers (Kita and Minami rivers) were 72.5 and 73.6 dpm/L, respectively, so we used the mean value of 73.1 dpm/L as the endmember for river water. The mean concentrations of ^{222}Rn in the terrestrial groundwater and the seawater outside the bay were 660 dpm/L. The salinity of the river water and terrestrial groundwater was assumed to be zero, all according to Sugimoto et al. (2016). The ^{222}Rn concentration and salinity at 0.9 m under the seabed at the station were determined to be 54.2 ± 23.5 dpm/L and 31.3 by direct measurement (Sugimoto et al. 2017, unpublished data), so we used a value of 54 dpm/L as the endmember for RSGD.

Half the plots in Fig. 11b are located above the mixing curve between seawater outside the bay (SW) and river water (RW), suggesting that the local SGD contributed to the ^{222}Rn concentration, whereas the major component of SGD, either terrestrial groundwater (tGW) or recirculated submarine groundwater (RSGD), could not be determined. In contrast, the daily changes in the ^{222}Rn concentration were in response to changes in wind direction. The concentration of ^{222}Rn was relatively high on 30 April–1 May, the period in which northward wind was dominant, whereas the ^{222}Rn concentration gradually

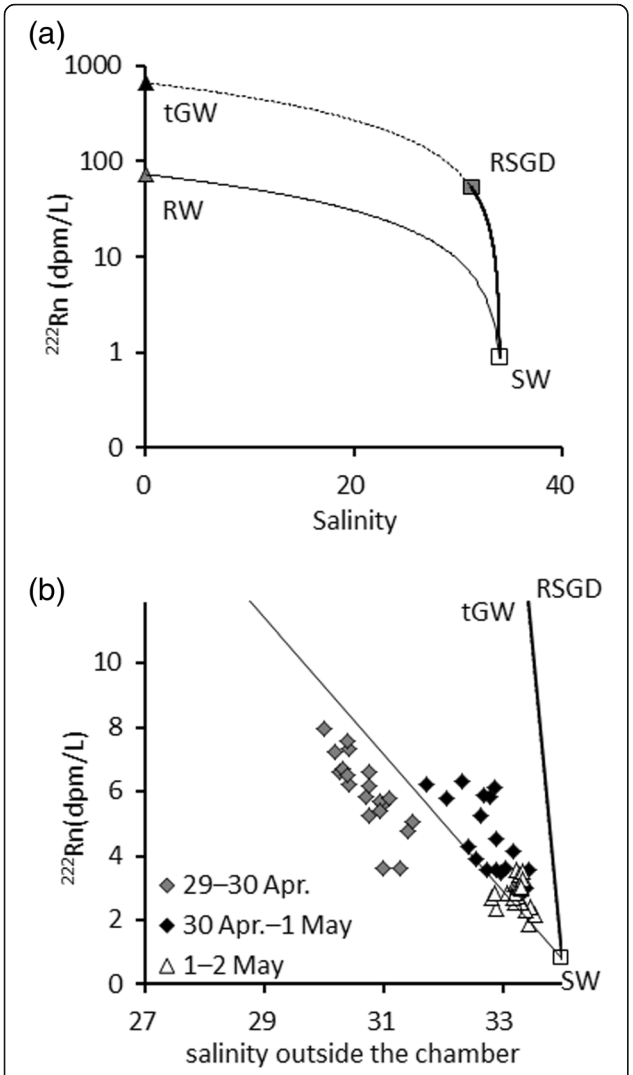

Fig. 11 **a** ^{222}Rn concentration (dpm/L) and salinity of the endmembers for seawater (*SW*), river water (*RW*), terrestrial groundwater (*tGW*), and recirculated submarine groundwater (*RSGD*). The *solid line*, *dotted line*, and *bold line* are the mixing curves between SW and RW, SW and tGW, and SW and RSGD, respectively. **b** Average ^{222}Rn concentration (dpm/L) for 1 h in each day plotted against salinity outside the chamber. The symbols RW, tGW, and RSGD indicate a part of each mixing curve

decreased on 1–2 May and became close to the endmember of SW on 2–3 May, the period in which the southward wind was dominant (Fig. 11b). These results provide evidence of the advection of high-^{222}Rn water, which was controlled mainly by the wind during the observation period. Moreover, as shown in Fig. 7, high-^{222}Rn and high-PO_4 seawater was present around the mouths of the Kita and Minami rivers (the zone between C and D, shown in Fig. 1b). This water moved northward when the northern wind became strong, supplying ^{222}Rn and PO_4 to the station at which the temporal variations in these parameters were measured.

The results of our various observations, including those made with seepage meters, the continuous monitoring of ^{222}Rn concentrations at a single station, and the monitoring survey of ^{222}Rn concentrations from a boat, together with measurements of the biogeochemical properties, suggest that the advection of high-^{222}Rn water plays an important role in controlling the temporal changes in the ^{222}Rn concentration at the station in the zone between B and C, whereas the local SGD might be another source of ^{222}Rn in the period when significant SGD flux was observed. The mass balance model (Burnett et al. 2008), which estimates SGD fluxes using ^{222}Rn records from monitoring surveys, could not be applied because the temporal changes in the advection of high-^{222}Rn water were significant.

Influence of SGD on the biogeochemical environment along the coastline

The results of the monitoring survey along the coastline suggest that groundwater, which is characterized by high ^{222}Rn, contributes to the nutrient supply in the bay. The N:P:Si molar ratio of the fresh groundwater on land was approximately 26:1:27, whereas that in the river water was 82:1:150 (Sugimoto et al. 2016), suggesting the groundwater is rich in PO_4. The concentrations of PO_4 and ^{222}Rn were both highest along the coastline in the zone between C and D (Fig. 7) and varied simultaneously (Fig. 10). This mutual correlation suggests that nutrients are supplied by SGD to the surface layer along the coastline.

The factors limiting primary productivity are listed in Table 2. The limitation factors for the maximum and minimum temperatures at each observation point (F_T) were nearly 1.0 in June, July, and September, suggesting that temperature was not a limiting factor in these seasons. F_T in March ranged from 0.64 to 0.81, indicating that temperature was one of the factors limiting primary productivity. Of the factors limiting primary productivity

Table 2 Maximum and minimum temperatures and concentrations of nutrients along the monitoring line shown by the dotted line in Fig. 1b in each month and limiting factors (F_T, T_N) for primary productivity

		Temp. (°C)	F_T	NO_{2+3} (μM)	DIP (μM)	F_N
March	Max.	11.9	0.80	20.7	0.18	0.49
	Min.	8.1	0.64	0.4	0.00	0.00
June	Max.	23.3	1.00	1.9	0.21	0.53
	Min.	20.6	0.98	0.1	0.00	0.00
July	Max.	29.8	0.98	8.3	0.23	0.55
	Min.	27.5	1.00	0.1	0.08	0.05
September	Max.	28.9	0.99	3.8	0.18	0.49
	Min.	26.3	1.00	0.0	0.00	0.00

Max. maximum, *Min.* minimum, *Temp.* temperature

in the sea, light intensity was not considered in this study because of a lack of data. However, light intensity was assumed to rarely limit primary production at the surface, as inferred from the limitation factor for light measured at the bottom in the shallow zone of Obama Bay (Sugimoto et al. 2017). F_N values for the minimum concentrations of nutrients at each observation point were all nearly 0.0, and F_N values for the maximum concentrations were around 0.5, suggesting that nutrients were a major factor limiting primary production at all the observation points.

The correspondence and correlation between the concentrations of ^{222}Rn and Chl-a at the surface in June, July, and September (Fig. 6, Table 1) suggest that the nutrients supplied by SGD influenced the phytoplankton biomass. The correlation of these factors in March was not significant, mainly because not only nutrients limited primary production but also temperature and probably light intensity. Of course, it is important to consider the influence of the seawater residence time on the concentrations of both ^{222}Rn and Chl-a. Although the links among ^{222}Rn, nutrient supply, and primary production must be more fully clarified in future studies, the results of this survey provide persuasive evidence that SGD influences the phytoplankton biomass in Obama Bay, whereas the nutrient supply pathways are not limited to the local SGD but are also influenced by its advection.

Conclusions

In this study, we conducted high-resolution mapping and made time-series measurements of ^{222}Rn and the biogeochemical properties along the coastline, combined with SGD measurements made with seepage meters, to examine the influence of SGD on the biogeochemical environment in Obama Bay. Our results show that (1) the observed concentrations of ^{222}Rn along the coast of the bay indicate that groundwater affected the biogeochemical properties of the bay and was not limited to the local SGD; (2) ^{222}Rn flowing into the bay from rivers (in which groundwater seeps from the river bed) had a strong effect on the distribution of ^{222}Rn concentrations along the coast; (3) high-^{222}Rn water was always present around the river mouths, and the northward advection of the water affected the distribution of ^{222}Rn concentrations; and (4) the southward wind suppressed the advection of high-^{222}Rn water and was the main control on temporal variations in the ^{222}Rn concentration at a station located to the north of the Kita and Minami rivers. Although the effect of the residence time of the seawater on the correlation between the concentrations of ^{222}Rn and Chl-a must be clarified in a future study, the results of this study provide persuasive evidence that the nutrients supplied by SGD influence the phytoplankton biomass in Obama Bay.

Abbreviations

AMeDAS: Automated Meteorological Data Acquisition System; Chl-a: Chlorophyll-a; SGD: Submarine groundwater discharge

Acknowledgements

The observations made with seepage meters along a line extending from onshore to offshore were made in collaboration with Wakasa High School. We are indebted to the members of the diving club and their teachers, Dr. Yasuyuki Kosaka and Mr. Hiroaki Hirayama, and the headmaster of Wakasa High School for their assistance. We sincerely thank Mr. Teruhiko Nakajima and Mr. Tomohiro Kawashiro of Fukui Prefectural University for supporting the development and deployment of the seepage chambers and the ^{222}Rn monitoring at the fixed stations. We are grateful to the journal editors and three anonymous reviewers for their helpful comments and suggestions.

Funding

This work was performed with the support of the Research Project Human–Environmental Security in Asia-Pacific Ring of Fire: Water–Energy–Food Nexus (R-08-Init) at the Research Institute for Humanity and Nature (RHIN).

Authors' contributions

SK, RS, DT, OT, and JS conceived and designed the study. HH, YM, and MY performed the field observations and data analysis. SN collaborated with the corresponding author in the data analysis and discussion. MT collaborated with the authors in the planning of the field observations. All the authors have read and approved the final manuscript.

Competing interests

The authors declare that they have no competing interests.

Publisher's Note

Author details

[1]Field Science Education and Research Center, Kyoto University, Kitashirakawaoiwake, Sakyo-ku, Kyoto 606-8502, Japan. [2]Research Center for Marine Bioresources, Fukui Prefectural University, 49-8-2, Katsumi, Obama, Fukui 917-0116, Japan. [3]Research Institute for Humanity and Nature, 457-4, Kamigamo Motoyama, Kita-ku, Kyoto 603-8047, Japan. [4]Idea Consultants Co., 2-2-2, Hayabuchi, Tsuzuki-ku, Yokohama, Kanagawa 224-0025, Japan. [5]Graduate School of Biosphere Science, Hiroshima University, 1-4-4 Kagamiyama, Higashi-hiroshima, Hiroshima 739-8528, Japan. [6]Graduate School of Maritime Sciences, Kobe University, 5-1-1 Fukae-minami, Higashi-nada-ku, Kobe 658-0022, Japan.

Received: 30 May 2016 Accepted: 9 March 2017
Published online: 24 March 2017

References

Bruce JR (1925) The metabolism of shore-living dinoflagellates. Br J Exp Biol 2: 413–426

Burnett WC, Dulaiova H (2003) Estimating the dynamics of groundwater input into the coastal zone via continuous radon-222 measurements. J Environ Radioact 69:21–35

Burnett WC, Kim G, Lane-Smith DA (2001) Continuous monitor for assessment of 222Rn in the coastal ocean. J Radioanal Nucl Chem 249:167–172

Burnett WC, Aggarwal PK, Aureli A, Bokuniewicz H, Cable JE, Charette MA, Kontar E, Krupa S, Kulkarni KM, Loveless A, Moore WS, Oberdorfer JA, Oliveira J, Ozyurt N, Povince P, Privitera AMG, Rajar R, Ramessur RT, Scholten J, Stieglitz J, Taniguchi M, Turner JV (2006) Quantifying submarine groundwater discharge in the coastal zone via multiple methods. Sci Total Environ 367:498–543

Burnett WC, Peterson R, Moore WS, de Oliveira J (2008) Radon and radium isotopes as racers of submarine groundwater discharge—results from the Ubatuba, Brazil SGD assessment intercomparison. Estuarine Coastal Shelf Res 76:501–511

Cable JE, Burnett WC, Chanton JP, Weatherly GL (1996) Estimating groundwater discharge into the northeastern Gulf of Mexico using radon-222. Earth Planet Sci Lett 144:591–604

Campbell EE, Bate GC (1996) Groundwater as a possible controller of surf diatom biomass. Revista Chilena De Historia Natural 69(4):503–510

Dulaiova H, Peterson R, Burnett WC, Lane-Smith DA (2005) A multi-detector continuous monitor for assessment of Rn-222 in the coastal ocean. J Radioanal Nucl Chem 263:361–365
Ellins KK, Roman-Mas A, Lee R (1990) Using 222Rn to examine groundwater/surface discharge interaction in the Rio Grade, DeManati, Puerto Rico. J Hydrol 115:319
Gobler CJ, Sanudo-Wilhelmy SA (2001) Temporal variability of groundwater seepage and brown tide blooms in a Long Island embayment. Mar Ecol Prog Ser 217:299–309
Holmes RM, Aminot A, Kerouel R, Hooker BA, Peterson BJ (1999) A simple and precise method for measuring ammonium in marine and freshwater ecosystems. Can J Fish Aquat 56(10):1801–1808
Honda H, Sugimoto R, Kobayashi S, Tahara D, Tominaga O (2016) Temporal and spatial variation in primary production in Obama Bay. Bull Jpn Soc Fish Oceanogr 80(4):269–282
Hosono T, Ono M, Burnett WC, Tokunaga T, Taniguchi M, Akimichi T (2012) Spatial distribution of submarine groundwater discharge and associated nutrients within a local coastal area. Environ Sci Technol 46:5319–5326
Ishitobi T, Taniguchi M, Shimada J (2007) Estimations of groundwater discharge and changes in fresh-salt water interface by measurements of submarine groundwater discharge in the coastal zone. Ground Water 49(3):191–204 (in Japanese with English abstract)
Johannes RE (1980) The ecological significance of the submarine discharge of groundwater. Mar Ecol Prog Ser 3:365–373
Kohout FA, Kolipinski MC (1967) Biological zonation related to groundwater discharge along the shore of Biscayne Bay. Miami, Florida. In: Lauff G (ed) Estuaries, vol 83. AAAS Publ., Washington, D.C, pp 488–499
Laroche J, Nuzzi R, Waters R, Wyman K, Falkowski P, Wallace D (1997) Brown Tide blooms in Long Island's coastal waters linked to interannual variability in groundwater flow. Glob Chang Biol 3(5):397–410
Lee DR (1977) A device for measuring seepage flux in lakes and estuaries. Limnol Oceanogr 22:140–147
Miller D, Ullman C, William J (2004) Ecological consequences of ground water discharge to Delaware Bay, United States. Ground Water 42(7):959–970
Moore WS (1996) Large groundwater inputs to coastal waters by 226Ra enrichments. Nature 380:612–614
Nestler J (1977) A preliminary study of the sediment hydrology of a Georgia salt marsh using Rhodamine WT as a tracer. Southeastern Geol 18:265–271
Officer CB (1976) Physical oceanography in estuaries. John Wiley & Sons, New York, p 465
Rutkowski CM, Burnett WC, Iverson RL, Chanton JP (1999) The effect of groundwater seepage on nutrient delivery and seagrass distribution in the Northeastern Gulf of Mexico. Estuaries 22:1033–1040
Sanders JG (1979) The importance of salinity in determining the morphology and composition of algal mats. Bot Mar 22:159–162
Santos IR, Niencheski F, Burnett WC, Peterson R, Chanton JP, Andrade CFF, Milani IB, Schmidt A, Knoeller K (2008) Tracing anthropogenically driven groundwater discharge into a coastal lagoon from southern Brazil. J Hydrol 353:275–293
Sasajima S, Sakamoto K (1962) Subsurface geology and groundwater of Obama Plain, Fukui pref., central Japan. Part 2: groundwater of Obama Plain. Memoirs of the Faculty of Liberal Arts, University of Fukui. Ser. II Natural science (in Japanese with English abstract)
Shiokawa M, Yamaguchi A, Umezawa Y (2013) Estimation of groundwater-derived nutrient inputs into the west coast of Ariake Bay. Bull Coastal Oceanography 50(2):157–167 (in Japanese with English abstract)
Steel JH (1962) Environmental control of photosynthesis in the sea. Limnol Oceanogr 7:137–150
Stieglitz TC, Cook PG, Burnett WC (2010) Inferring coastal processes from regional-scale mapping of 222Radon and salinity: examples from the Great Barrier Reef, Australia. J Environ Radioact 101:544–552
Sugimoto R, Honda H, Kobayashi S, Takao Y, Tahara D, Tominaga O, Taniguchi M (2016) Seasonal changes in submarine groundwater discharge and associated nutrient transport into a tideless semi-enclosed embayment (Obama Bay, Japan). Estuar Coasts 39:13–26
Sugimoto R, Kitagawa K, Nishi S, Honda H, Yamada M, Kobayashi S, Shoji J, Ohsawa S, Taniguchi M, Tominaga O (2017) Phytoplankton primary productivity around submarine groundwater discharge in nearshore coasts. Mar Ecol Prog Ser 563:25–33
Taniguchi M (2002a) Tidal effects on submarine groundwater discharge into the ocean. Geophysical Res Lett 29(12). doi:10.1029/2002GL014987
Taniguchi M, Iwakawa H (2004) Submarine groundwater discharge in Osaka Bay, Japan. Limnology 5:25–32
Taniguchi M, Burnett WC, Cable JE, Turner JV (2002) Investigation of submarine groundwater discharge. Hydrol Process 16:2115–2129
Valiela I, Costa JE (1988) Eutrophication of Buttermilk Bay, a cape cod coastal embayment: concentrations of nutrients and watershed nutrient budgets. Environ Manag 12(4):539–553
Valiela I, Foreman K, LaMontagne M, Hersh D, Costa J, Peckol P, DeMeo-Andreson B, D'Avanzo C, Babione M, Sham C, Brawley J, Lajtha K (1992) Couplings of watersheds and coastal waters: sources and consequences of nutrients enrichment in Waquoit Bay, Massachusetts. Estuaries 15:443–457
Waska H (2011) Submarine groundwater discharge (SGD) as a main nutrient source for benthic and water-column primary production in a large intertidal environment of the Yellow Sea. J Sea Res 65(1):103–113
Waska H, Kim G (2010) Differences in microphytobenthos and macrofaunal abundances associated with groundwater discharge in the intertidal zone. Mar Ecol Prog Ser 407:159–172
Yanagi T, Onitsuka G (1999) Numerical model on the lower trophic level ecosystem in Hakata Bay. Umi-no-Kenkyu 8:245–251 (in Japanese with English abstract)